Stochastic climate models, Part II
Application to sea-surface temperature anomalies and thermocline variability

By CLAUDE FRANKIGNOUL[1] and KLAUS HASSELMANN, *Max-Planck-Institut für Meteorologie, Bundesstr. 55, 2000 Hamburg 13, FGR*

ABSTRACT

The concept of stochastic climate models developed in Part I of this series (Hasselmann, 1976) is applied to the investigation of the low frequency variability of the upper ocean. It is shown that large-scale, long-time sea surface temperature (SST) anomalies may be explained naturally as the response of the oceanic surface layers to short-time-scale atmospheric forcing. The white-noise spectrum of the atmospheric input produces a red response spectrum, with most of the variance concentrated in very long periods. Without stabilizing negative feedback, the oceanic response would be nonstationary, the total SST variance growing indefinitely with time. With negative feedback, the response is asymptotically stationary. These effects are illustrated through numerical experiments with a very simple ocean-atmosphere model. The model reproduces the principal features and orders of magnitude of the observed SST anomalies in mid-latitudes. Independent support of the stochastic forcing model is provided by direct comparisons of observed sensible and latent heat flux spectra with SST anomaly spectra, and also by the structure of the cross correlation functions of atmospheric surface pressure and SST anomaly patterns. The numerical model is further used to simulate anomalies in the near-surface thermocline through Ekman pumping driven by the curl of the wind stress. The results suggest that short-time-scale atmospheric forcing should be regarded as a possible candidate for the origin of large-scale, low-period variability in the seasonal thermocline.

1. Introduction

In Part I of this series (Hasselmann, 1976, referred to in the following as I) a stochastic model of climate variability was considered in which slow changes of climate were interpreted as the integral response to continuous random excitation by short-time-scale "weather" disturbances. To illustrate the basic concepts of the model we consider here a very simple "climatic system" consisting only of the upper layer of the ocean, which is driven by the random fluxes of heat and momentum across the air–sea interface. The model reproduces the principal features and orders of magnitude of observed mid-latitude sea surface temperature (SST) variability in the period range of approximately one

_____
[1] Present address: Department of Meteorology, Massachusetts Institute of Technology, Cambridge, MA02139, U.S.A.

month to two years, and is not inconsistent with the observed thermocline variability in the period range of a few weeks to half a year. In view of its strong simplifications the model should nevertheless be viewed only as an example of the basic statistical structure which may be expected generally for a two-time-scale climatic system, rather than an attempt to model quantitatively the upper layers of the ocean. A number of models of the internal dynamics of the upper layers of the ocean have been proposed, most of them more sophisticated than the one considered here (cf. Niiler, 1975 or Thompson, 1976 for reviews), but the principal features of the input-response relations with which we shall be concerned are independent of the details of the model. Another very simple climatic model applicable for longer time scales in the range 1 to 10^5 years is discussed in Part III of this series (Lemke, 1977).

Because of their long persistence, large-scale SST anomalies have attracted considerable attention in the context of long-range weather forecasting. Strong indications of SST-weather relationships have been revealed through the statistical analyses of extended time series (cf. Bjerknes, 1966; Namias, 1969). Numerical experiments have also clearly demonstrated statistically significant modifications of weather patterns by critically placed SST anomalies, particularly in the tropics (e.g. Shukla, 1975; Rowntree, 1976), although the effects in mid-latitudes are often more difficult to detect in the presence of the higher natural variability of the atmosphere (Salmon & Hendershott, 1976; Chervin et al. 1976).

Since anomalous thermal or circulation patterns in either the ocean or the atmosphere may significantly modify the conditions in the other medium, it has often been suggested that SST anomalies arise through ocean-atmosphere feedback processes, in which the presence of an SST anomaly modifies the weather patterns in such a manner that the anomaly is strengthened (e.g. Namias, 1959, 1969)—although in some situations the atmosphere may also tend to destroy an existing SST anomaly (Namias, 1975). We suggest here that the development of SST anomalies can be understood more simply, without invoking feedback mechanisms, as the integral response of the ocean to random short-time-scale forcing by the atmosphere—in accordance with an earlier proposal by Mitchell (1966).

Following the notation of I, the heat balance equation governing the evolution of an SST anomaly $y(t)$ at a given position in the ocean (or defined as an areal average) is assumed to have the simple form

$$\frac{dy}{dt} = v(y, \mathbf{x}(t)) \qquad (1.1)$$

where v is a forcing function determined by the fluxes of latent and sensible heat, short- and long-wave radiation and momentum across the air–sea interface. The forcing function is regarded as parameterized in terms of various atmospheric boundary-layer variables $\mathbf{x}(t)$ and mixed-layer parameters. For simplicity, we shall retain only the SST anomaly as mixed-layer parameter in v (cf. Section 3).

The basic assumption of the stochastic forcing model in I is that the characteristic correlation time

scale τ_x of the atmospheric variables $x(t)$ is small compared with the time scale τ_y of the response $y(t)$. For integration times $t \ll \tau_y$, the variable y can then be regarded as constant in the right-hand side of (1.1), and the evolution of the SST change $\delta y(t) = y(t) - y_0$ relative to an initial temperature $y = y_0$ at time $t = 0$ is given by the equation

$$\frac{d}{dt}\, \delta y = v(y_0, \mathbf{x}(t)) = v(t) \qquad (1.2)$$

where $v(t)$ may be regarded as a given, random function of t. Dividing the variables into mean and fluctuating components, $\delta y = \langle \delta y \rangle + y'$, $v = \langle v \rangle + v'$ where the means $\langle \ldots \rangle$ are defined as ensemble averages over the atmospheric states x for given y_0, eq. (1.2) may then be divided into a mean part and a fluctuating part, given by

$$\frac{dy'}{dt} = v'(t) \qquad (1.3)$$

Equation (1.3) corresponds to the well-known continuous random-walk equation first considered by Taylor (1921). For a statistically stationary input $v'(t)$ the response is nonstationary, the variance of y' increasing linearly with time for $t \gg \tau_x$

$$\langle y'^2 \rangle = 2\, Dt \quad \text{for } \tau_x \ll t \ll \tau_y \qquad (1.4)$$

where the diffusion coefficient $D = \frac{1}{2}\int_{-\infty}^{\infty} R(\tau)$, and $R(\tau) = \langle v'(t + \tau)\, v'(t) \rangle$ denotes the input covariance function.

The variance spectra $F(\omega)$ of the input v' and $G(\omega)$ of the response y' are related in the corresponding frequency intervals through

$$G(\omega) = \frac{F(\omega)}{\omega^2} \approx \frac{F(0)}{\omega^2} \quad \text{for } \tau_y^{-1} \ll \omega \ll \tau_x^{-1} \qquad (1.5)$$

The non-integrable singularity of the response spectrum (1.5) at $\omega = 0$ is consistent with the non-stationarity of y. For large $t \gg \tau_x$, the variance of y' is contained almost entirely in a linearly growing δ-function at zero frequency. In accordance with the spectral interpretation of (1.4), the diffusion coefficient can be expressed rather simply in terms of the spectral density of the input at zero frequency,

$$D = \pi F(0) \qquad (1.6)$$

The input spectrum is white in the range $\tau_y^{-1} \ll \omega \ll$

τ_x^{-1}, and the spectrum $F(0)$ at zero frequency in eqs. (1.5) and (1.6) should in fact be interpreted more rigorously as referring to this band, since the side condition $t \ll \tau_y$ precludes a meaningful definition of the spectrum for frequencies of order τ_y^{-1} or less.

For $t = 0(\tau_y)$, y can no longer be regarded as constant in the right-hand side of (1.2) and (1.3), and feedback effects become important. A net positive feedback converts the linear growth in the range $\tau_x \ll t \ll \tau_y$ into an exponential instability, and can therefore be ruled out as a realistic possibility. Negative feedback, however, leads to an asymptotic balance between the random forcing and the feedback damping, yielding a statistically stationary response. For the simplest case of a linear feedback, eq. (1.1) takes the form

$$\frac{dy}{dt} = v(t) - \lambda y \quad \lambda > 0, \text{const.} \qquad (1.7)$$

and the structure function

$$[\delta y^2(t)] = [(y(t_0 + t) - y(t_0))^2]$$

of the response is given by

$$[\delta y^2] = \frac{2D}{\lambda} (1 - e^{-\lambda t}) \quad \text{for } t \gg \tau_x \qquad (1.8)$$

Ensemble values over all y and x (corresponding to time averages over periods $\tau \gg \tau_y$) have been denoted here by square brackets [...] to distinguish them from the ensemble values $\langle ... \rangle$ over x for fixed y (which correspond to time averages over intermediate periods satisfying $\tau_x \ll T \ll \tau_y$). The equivalent spectral relations to (1.8) are given by

$$G(\omega) = \frac{F(0)}{\omega^2 + \lambda^2} \quad \text{for } \omega \ll \tau_x^{-1} \qquad (1.9)$$

An important feature of eqs. (1.8) and (1.9) is that, although the atmospheric forcing can be regarded as essentially uncorrelated white noise, the SST correlation time scale is very much larger, being determined solely by the relaxation time arising from the linear feedback.

We apply these stochastic forcing concepts now to a very simple SST model in which the upper layer of the ocean is represented by a mixed layer

of fixed depth ("copper plate" model). The concept is tested both numerically, in a Monte-Carlo simulation using a simple two-dimensional turbulent model atmosphere (Sections 2 and 3), and against real input and response data (Section 4). In general it is found that the atmospheric input anomaly spectra are white in the relevant period range from a few weeks to a few years, as required, and that the SST spectra conform with the predicted form (1.9). Despite the crude copper-plate model of the mixed layer, the orders of magnitude of the input and response spectra are also in reasonable agreement with theory.

In Section 5 the stochastic forcing model is applied to variability in the seasonal thermocline. In this case the driving term is the Ekman suction produced by the curl of the wind stress. For periods shorter than about 6 months, the β-effect does not play a role, so that the linear response of the mixed layer can be characterized by an equation of the form (1.1), and a time-scale separation between input and response is again possible. Comparison of the model simulations with observations suggest that the short-term random wind forcing may yield a non-negligible contribution to the variability of the seasonal thermocline. However, quantitative comparisons are more difficult in this case because of inadequate observational data on the wavenumber-frequency spectra of the wind-stress curl.

2. The atmospheric model

Random atmospheric forcing is simulated in our numerical stochastic air–sea interaction model using a barotropic model of quasi-geostrophic turbulence, in a form developed by Kruse (1975) for numerical investigations of the nonlinear transfer within large-scale atmospheric motions in an equilibrium state. The model is of the type discussed, for example, by Lilly (1972) and Rhines (1975). It provides a statistically stationary wind field, from which heat and momentum anomaly fluxes are inferred using bulk transfer formulae. The atmospheric system is not affected by the underlying oceans, i.e. there is no direct feedback from the ocean to the atmosphere.

Kruse's model represents a non-divergent, one-layer atmosphere in the β-plane approximation, bounded by two latitudes and zonally cyclic. The dependent variable is the stream function which

obeys the equation

$$\frac{d}{dt} \nabla^2 \psi + J(\psi, \nabla^2 \psi) + \beta \frac{\partial \psi}{\partial x} = \text{forcing} + \mu \nabla^4 \psi -$$

$$-r \nabla^2 \psi \qquad (2.1)$$

where

$$\frac{d}{dt} = \frac{\partial}{\partial t} + U_0 \frac{\partial}{\partial x}$$

Here x and y are eastward and northward Cartesian coordinates, U_0 a constant velocity taken to be 5 m sec^{-1}, and J denotes the Jacobian operator. The dissipation terms simulate a combination of internal viscous friction and surface drag. The boundary conditions are

$$v = \frac{\partial \psi}{\partial x} = 0 \quad \text{at } y = 0, L_y \qquad (2.2)$$

and

$$\psi(x, y, t) = \psi(x \pm pL_x, y, t) \quad p = 1, 2, \ldots \qquad (2.3)$$

It is assumed in the following that $L_x = L_y = 8800$ km ("hemispheric model"). Equations (2.1)–(2.3) are solved spectrally by expanding Ψ in terms of harmonic functions. In our numerical experiments the series is square truncated after wavenumber 8. Wavenumber k in the model corresponds to longitudinal wavenumber $n \simeq 4k$ in the atmosphere. The flow is assumed to be symmetric about 45° latitude ($y = L_y/2$) to reflect the mid-latitude maximum of eddy kinetic energy (this also has the advantage of reducing the number of Fourier coefficients). A constant forcing is imposed at wavenumbers (2,3) and (3,2) to simulate baroclinic instability. The prognostic equations for the Fourier amplitudes were solved by alternating a Baer–Platzman and an Adams–Bashfort time-stepping scheme with a time step of 1 h.

After the wind field had reached an approximate steady state (characterized by constant energy and enstrophy spectra), the equations were stepped for a further period of 512 simulated days. Fourier amplitudes were saved at 12-h intervals only, since there was little energy at frequencies higher than a cycle per day. The wind field was constructed on a 16 × 16 grid by inverse Fourier transformation.

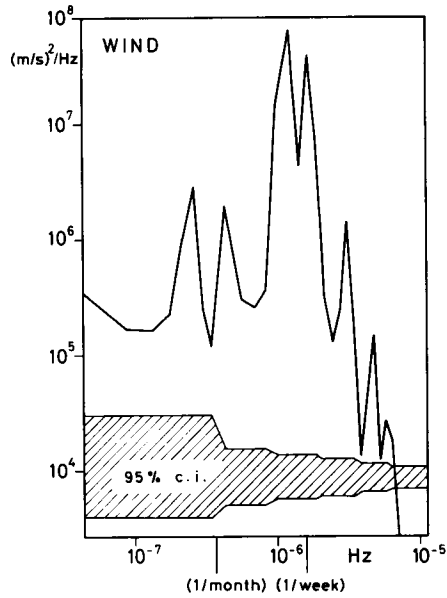Fig. 1 shows the power spectrum of the simulated wind data. The general features of

Fig. 1. Simulated spectrum of the wind velocity at $x = 0$, $y = L_y/4$.

observed wind spectra are reproduced: a constant energy level at low frequencies, a peak at periods of several days, and a strong drop off at higher frequencies. Nevertheless, compared with observed wind spectra above the ocean (Byshev & Ivanov, 1969; Wunsch, 1972; Frost, 1975), the simulated spectrum is nearly one order of magnitude too small at low frequencies and the energy peak is nearly one order of magnitude too high. However, this deficiency can be readily corrected for when comparing our computed oceanic response spectra against observations, since the input-response relations are linear. The wavenumber spectrum of the wind (Fig. 2) reproduces reasonably well wavenumber spectra observed in the troposphere (for example by Kao & Wendell, 1970), although observations suggest a somewhat flatter spectrum at low wavenumbers and a less steep decay proportional to k^{-3} at high wavenumbers. This latter discrepancy arises from the rather strong dissipation and limited wavenumber range of the model, which prevents the formation of an enstrophy inertial range. It should also be pointed out that the model wavenumber spectrum may show additional deficiencies when applied to the marine boundary layer.

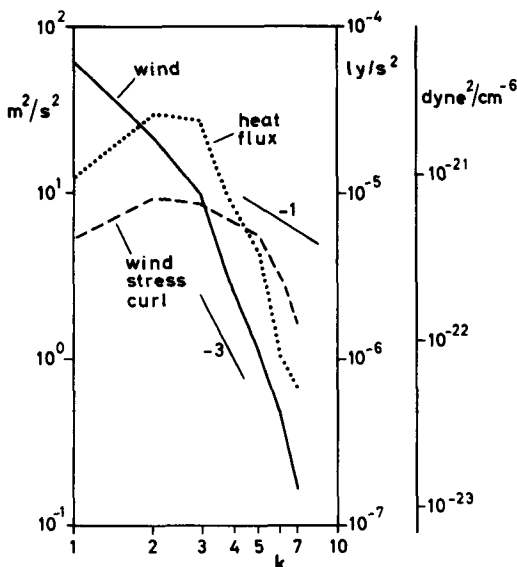Despite its oversimplifications, the atmospheric model provides a simulation of a statistically

Fig. 2. Simulated wavenumber spectrum of wind velocity (continuous lines), total heat flux (dotted line) and wind-stress curl (dashed lines). The values are averages over eight independent estimates.

stationary wind field which is not too unrealistic. From the wind field, the heat and momentum anomaly fluxes which drive the ocean can then be calculated using bulk transfer formulae (Section 3). The main advantage of using a numerical model to simulate the forcing rather than observed data is that one obtains in this way a complete three-dimensional spectral description of the forcing functions with respect to frequency and horizontal wavenumber, and this is difficult to extract from real data.

3. Simulated sea surface temperature anomalies

(a) The mixed-layer model

The simplest models of the uppermost layer of the ocean assume a completely mixed, horizontally homogeneous layer of depth h and temperature T overlying a seasonal thermocline with prescribed temperature structure (e.g. Kraus & Turner, 1967; Denman, 1973; Niiler, 1975; Thompson, 1976). Ignoring the effects of salinity and horizontal advection, the evolution of the layer parameters h, T are then governed by two prognostic equations of

the form

$$\frac{d(hT)}{dt} = f_1 (T, T_a, q, \mathbf{U}, R) \tag{3.1}$$

$$\frac{dh}{dt} = f_2 (\mathbf{U}) \tag{3.2}$$

Equation (3.1) is a heat balance equation in which f_1 denotes the sum of (a) the total flux of latent heat H_L and sensible heat H_s through the air–sea interface (dependent on the air temperature T_a, humidity q and wind speed U through the standard bulk transfer relations), (b) the net short- and longwave radiation R through the sea surface, and (c) the heat exchanged with the layer below. The second equation (3.2) is an empirical relation based on an energy argument in which it is postulated that a fixed (small) fraction of the turbulent energy produced in the mixed layer is used to thicken the layer by entrainment of fluid from below. It is normally assumed that the kinetic energy converted into potential energy by the entrainment process is supplied to the mixed layer by the wind, so that the source function f_2 depends only on the wind speed (apart from internal parameters of the system such as the stratification of the thermocline).

We shall simplify this model further by retaining only eq. (3.1) and assuming that the mixed-layer depth remains constant. In addition, only the contribution (a) to f_1 will be considered. The variations in radiation flux (b) are ignored, since they cannot be incorporated in our simple atmospheric model, and the neglect of the heat exchange (c) with the lower layer is consistent with the neglect of entrainment. If we apply the usual bulk transfer relations, we may then parameterize f_1 in the form

$$f_1 = (H_s + H_L) (\rho^w C_p^w)^{-1} \tag{3.3}$$

where

$$H_s + H_L = C_H(1 + B)\rho^a C_p^a(T_a - T)|\mathbf{U}| \tag{3.4}$$

and C_H is the bulk transfer coefficient for the sensible heat flux, B the (Bowen) ratio of the latent heat flux to the sensible heat flux, ρ^a and ρ^w the densities of air and water, and C_p^a and C_p^w the specific heats of air and water.
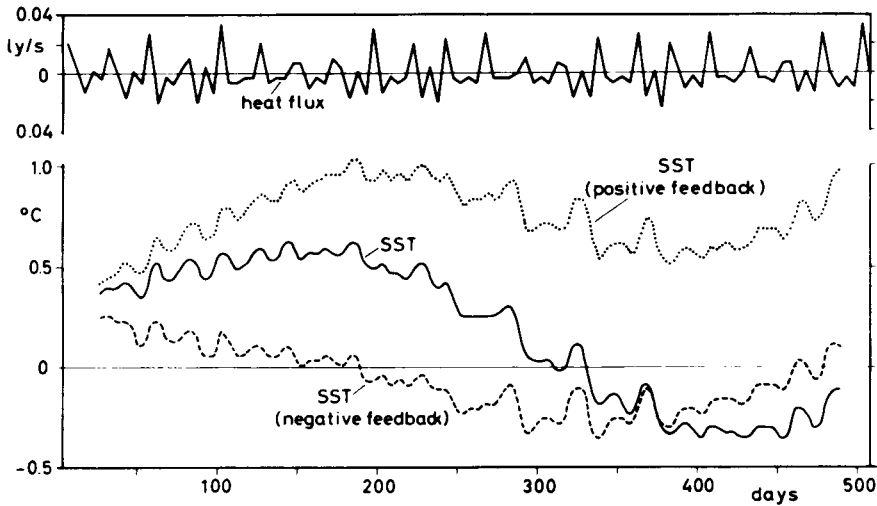
Fig. 3. Simulated SST variations (without and with feedback effect) and total heat flux at $x = 0$, $y = L_y/4$. The heat flux time series is subsampled at 5-day intervals and the SST time series are low-passed, using a quadratic Lanczos filter (cut-off frequency $8 \cdot 10^{-7}$ Hz).
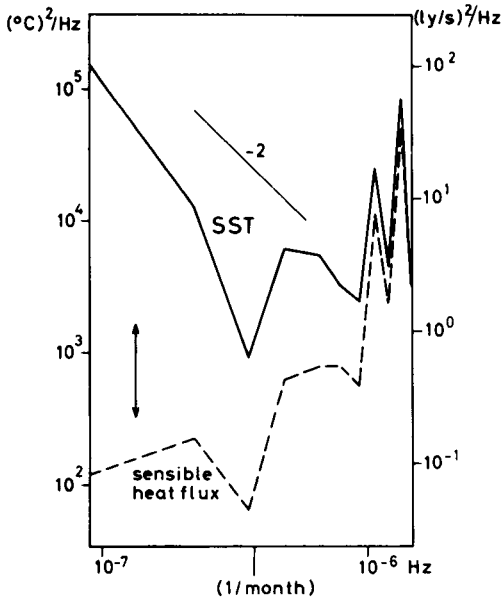

Fig. 4. Simulated spectrum of sensible heat flux (dashed lines) and SST anomaly (continuous lines) at $x = 0$, $y = L_y/4$. The arrows indicate the 95% confidence interval.

To incorporate heat transfer into our atmospheric model we assume that the air–sea temperature difference is proportional to the north–south velocity V, $(T_a - T) = KV$, $K = $ const. Thus when the wind blows from the north, the water

cools, and when it blows from the south, the water warms. With this crude parameterization an equation formally analogous to eq. (1.1) is obtained for the rate of change of SST,

$$\frac{dT}{dt} = C_H \left(1 + B\right) \frac{\rho^a \, c_p^a \, KV|U|}{\rho^w \, c_p^w \, h} \tag{3.5}$$

In our simulations, we have set $K = 0.25$ (° C/m/s) and taken $C_H = 10^{-3}$, $B = 3$, $\rho^a = 1.25 \ 10^{-3}$ gm cm^{-3}, $\rho^w = 1$ gm cm^{-3}, $C_p^a = 0.24$ cal gm^{-1} (° C)$^{-1}$, $C_p^w = 0.96$ cal gm^{-1} (° C)$^{-1}$, and $h = 25$ m. A mixed-layer depth of 25 m has been suggested by Thompson (1976) for low mid-latitudes (30° N) on the basis of a comparison of the observed seasonal SST cycle with predictions by a copper-plate model. The effective mixed-layer depths at higher latitudes are considerably greater (a value of 100 m is taken in the following section for station India at 59° N). With our choice of K, the r.m.s. air–sea temperature difference generated by the model is 1.25 °C.

(b) *Simulated SST anomalies neglecting feedback*

Time series of the stochastic atmospheric forcing according to eq. (3.5) were constructed at each grid point, and the SST changes were then calculated by straightforward integration. Fig. 3 illustrates the integral response of the SST to the rapidly varying fluxes. To draw attention to the evolution of the low frequencies in the SST fluctuations, the SST time

series have been low-pass filtered. The longer the integration time in (3.5), the larger the amplitude of the SST oscillations, as expected from the non-stationarity state of the climatic response for the case without feedback.

The power spectrum of the simulated sensible heat flux anomaly at a fixed location is shown in Fig. 4. It has the same features as the simulated wind spectrum (Fig. 1). In particular, it is essentially white at low frequencies, in agreement with observation (and as required by theory) although the energy level is about one order of magnitude lower than observed flux data (Section '4). The simulated flux spectrum implies a diffusion coefficient according to relation (3.5) of $D \approx 0.25$ $(°C)^2$ year^{-1}, i.e. the random atmospheric forcing produces a standard deviation in the SST of about 0.7 °C in one year. As predicted by relation (1.5), the simulated SST anomaly spectrum is proportional to the inverse frequency squared at low frequencies (Fig. 4). This is again in agreement with the observations, and the energy level is also about one order of magnitude lower than observed mid- and high-latitude levels, in accordance with the order of magnitude underestimate of the simulated input spectrum. A more detailed comparison with the observations is given in Section 4.

The wavenumber spectrum of the SST anomalies is proportional to the wavenumber spectrum of the atmospheric input (Fig. 2, dotted lines). In contrast to the wind spectrum, which is highest at wavenumber 1, the maximum variance of the simulated SST occurs at wavenumbers 2 and 3. This corresponds roughly to the observed scale of the dominant SST anomaly patterns, which are typically several thousand kilometers in diameter, and is also consistent with the observation that the dominant scales of the SST anomalies appear to be somewhat smaller than the scales of air temperature or sea-level pressure anomalies (e.g. Kraus & Morrison, 1966; Davis, 1976).

Although our ocean-atmosphere model is admittedly highly simplified, the main features of the SST spectral response to short time scale weather forcing appear to be reproduced reasonably well in the numerical experiments. As discussed in Section 4, further processes (e.g. radiation fluxes of Ekman transport) will need to be considered in more quantitative models. However, as long as these can be represented by short-time-scale "weather variables", they will yield only an additional white noise input. Depending on their correlation with the

sensible and latent heat fluxes considered here, they will produce lower or higher energy levels of the SST anomalies, but no changes in the basic structure of the spectrum. Other effects which should be incorporated in more detailed models include slow changes in the coupled system (e.g. seasonal variations of the mixed-layer depth), which will modulate the oceanic response.

Up to this point we have also omitted feedback effects. The observations (Section 4) suggest that the characteristic feedback time of SST anomalies is of the order of 6 months, so that the results of this section can be applied only for periods shorter than this time scale.

(c) Simulated SST anomalies including feedback

For small temperature anomalies, the function f_1 in eq. (3.1), $dT/dt = f_1/h$ ($h = $ const), can be expanded with respect to T. Writing $f_1 = [f_1] + f_1'$, and defining $T = 0$ to correspond to an equilibrium temperature for which $[f_1] = 0$, eq. (3.1) then takes the form of a first-order autoregressive (Markov) process

$$\frac{dT}{dt} = \frac{f_1'}{h} - \lambda T \qquad (3.6)$$

where $\lambda = (\partial [f_1]/\partial T)_{T=0}$ is a constant feedback factor. For a stable system with negative feedback, λ is positive (cf. eq.) (1.7)).

Since our atmospheric model contains no thermodynamics, we cannot simulate the feedback explicitly in the coupled system. However, we can estimate the feedback factor by expanding the bulk formula (3.4) with respect to T. Assuming the air temperature to remain constant, this yields

$$\lambda = \rho^a C_p^a (\rho^w C_p^w)^{-1} C_H (1 + B) \langle |U| \rangle h^{-1} \qquad (3.7)$$

where $\langle |U| \rangle$ is the mean wind speed. Taking $\langle |U| \rangle = 8$ m sec^{-1} and C_H, B and h as given in Section 3a, one obtains $\lambda = (1.7$ month$)^{-1}$. This feedback factor is larger than inferred from observations, presumably because of the unrealistic assumption of a constant air temperature (cf. Section 4). The value was nevertheless used in our model experiments to illustrate the stabilizing influence of a negative feedback in our rather short (512) day simulation runs (Fig. 3). The decrease in amplitude of the lowest frequency SST oscillation as compared with the case without feedback is clearly dis-

cernible. The computed SST spectra also showed a corresponding flattening at low frequencies, as expected.

Our simulation experiments may be compared with the work of Salmon & Hendershott (1976), who simulated one year of air–sea interaction processes by coupling a two-layer, thermally variable atmospheric model to a "copper plate" oceanic mixed layer. With this more realistic model, which simulated the observed northern hemisphere seasonal cycle in fair detail, they found a frequency spectrum of SST anomaly very similar to the spectrum represented in Fig. 4. This supports the premise that the principal features of the SST variability are independent of the details of the coupling and can be inferred from the general concept of a white forcing spectrum and a linear auto-regressive integrator response, with a large time-constant separation between input and response.

For comparison, Fig. 3 also shows the characteristic "explosive" behaviour of the processes with linear positive feedback, $\lambda < 0$. Because of the short time scales involved, this case can be ruled out for SST anomalies, but it has been suggested that it may be relevant for more inert components of the climatic system, such as the ice sheets. It should be noted that a positive linear feedback does not necessarily imply overall climate instability, as non-linear terms can stabilize the response at larger amplitudes.

4. Comparison with observations

The principal features of the stochastic two-scale model of SST variability are that the frequency spectra of SST anomalies obey an inverse square law for frequencies in the range $\tau_y^{-1} \ll \omega \ll \tau_x^{-1}$, flattening to a constant level at lower frequencies, and that the atmospheric input spectra are white throughout this frequency range. Examples of data exhibiting these features are given in Figs. 5 and 6.

Fig. 5 shows the spectra of SST anomaly at the Atlantic Ocean weather ship India (59° N, 19° W), and Fig. 6 shows the spectra of latent and sensible heat flux at the same location (after Frost, 1975). The seasonal signal has been subtracted from the SST time series, but not from the latent and sensible heat flux series. Approximately 16 years of
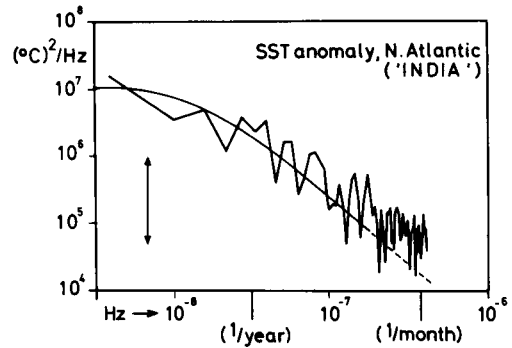
Fig. 5. Spectrum of SST anomaly at Ocean Weather Ship India for the period 1949–1964 (after Frost, 1975). The arrows indicate the 95% confidence interval. The smooth curve was calculated from relation (4.1) with $h = 100$ m, $\lambda = (4.5 \text{ month})^{-1}$.
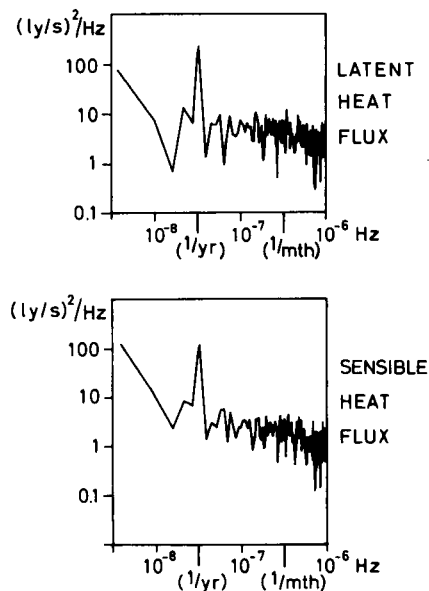
Fig. 6. Spectra of latent and sensible heat flux at Ocean Weather Ship India for the period 1949–1964 (after Frost, 1975).

data were available, and the SST anomaly spectrum was computed from 14-day average data, yielding a Nyqvist frequency of about 1 cycle per month. Daily averages of the fluxes were computed from the flux time series obtained from the three hourly wind and temperature data using the bulk formulae, thereby avoiding the usual difficulties of estimating fluxes from climatologically averaged wind and temperature fields.

Both the SST spectra and the flux spectra agree well with the form predicted by theory. The flattening of the SST spectra at high frequencies may be attributed to aliasing. The flattening at low frequencies corresponds to a linear feedback factor $\lambda = (4.5$ months$)^{-1}$. Kraus & Morrison (1966, Table 7) have calculated the correlation function $r_{TT}(\tau)$ of monthly average SST anomalies at station India from 12 corresponding years of data. Fitting a function $e^{-\lambda\tau}$ (predicted from eq. (1.7), see appendix) to the given values of $r_{TT}(\tau)$ also gives good agreement for $\lambda = (4.5$ months$)^{-1}$. This feedback factor is smaller than the value $\lambda = (1.7$ months$)^{-1}$ which was computed in Section 3 from the bulk formula under the assumption that changes in SST were not accompanied by changes in air temperature. In fact it is known that the heat exchange across the sea surface rapidly leads to an adjustment of the surface air temperature to a value fairly close to the local SST, so that SST anomalies always produce air temperature anomalies of the same sign and only slightly smaller amplitude (cf. Thompson, 1976). Thus the net feedback factor, as determined by the true air–sea temperature difference in the bulk formula, may be expected to be considerably smaller than $\lambda = (1.7$ months$)^{-1}$.

The ratio of the latent and sensible heat flux spectra to the SST spectrum is also consistent with the simple copper-plate model described in the previous section. From (3.1) and (3.3) we find

$$G(\omega) = \frac{F_S(0) + F_L(0)}{h^2\,\rho^{w2}\,c_p^{w2}\,(\omega^2 + \lambda^2)} \qquad (4.1)$$

where $G(\omega)$ is the SST spectrum, and $F_S(0)$ and $F_L(0)$ are the (constant) low frequency levels of the sensible and latent heat flux spectra, respectively. At the high latitude of station India, these fluxes are likely to dominate the local heat balance, although radiation effects may be important in summer. Dimensional arguments (see also Gill & Niiler, 1973) suggest furthermore that heat advection by anomalous wind driven currents play a minor role in mid- and high latitudes. It has also been assumed here for simplicity that the sensible and latent heat flux variations are uncorrelated, which is probably incorrect, but the degree of correlation is unimportant, since $F_L(0) \gg F_S(0)$. Equation (4.1) is in agreement with the data if a value $h = 100$ m is chosen, which is consistent with typical depths of the seasonal thermocline at station India (Frost,
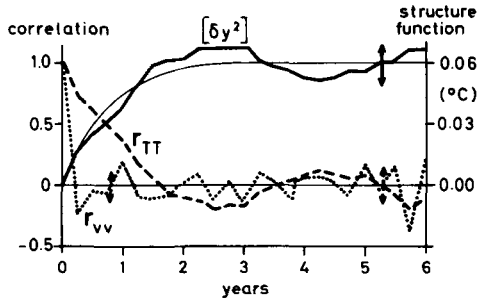

Fig. 7. ———: structure function $[\delta y^2(t)]$ of the North Pacific SST anomaly data of Namias (1969). ———: predicted structure function for $D = 0.04(^\circ\text{C})^2$ yr^{-1}, $\lambda = (0.75$ yr$)^{-1}$. −−−−: correlation function of the SST anomaly data. ....: input correlation function inferred from differenced temperature time series. The arrows indicate the variance of the correlation estimates (approximately $\frac{1}{2}$ the 95 % confidence intervals).

1975). The energy levels correspond to a diffusion coefficient (eqs. (1.4), (1.6)) of $D = 1.5(^\circ\text{C})^2$/yr, which means that without feedback the short-time-scale atmospheric flux variations would produce r.m.s. SST anomalies of order $(2 \cdot (1.5))^{1/2} = 1.7\,^\circ\text{C}$ in a year.

Another example of a local temperature variance spectrum, in this case for 13 years of data taken at 10-m depth at the Panulirus station near Bermuda (32° N, 65° W) can be found in Fig. 16 of Wunsch (1972). the seasonal signal was not removed, but the ω^{-2} behaviour of the spectrum for frequencies above 1 cpy is nevertheless apparent. The energy level is here also of the same order as at station India, but a quantitative comparison of the input–response energy levels is not possible in this case because the relevant input data was not given.

Figs. 7 and 8 show correlation (structure) functions and power spectra of spatially averaged SST anomalies and atmospheric pressure anomalies for the North Pacific. The structure function of Namias' (1969) 25-year time series of SST anomaly data, averaged over the entire Pacific north of 20° N, Fig. 7, shows initially a linear increase with lag, as predicted by the stochastic forcing model without feedback, followed by a flattening to a constant value, as expected when the stabilising feedback comes into play at large time lags (eqs. (1.4) and (1.8)). Continuous time series data for the integrated air–sea fluxes over the North Pacific are not available, but the equivalent
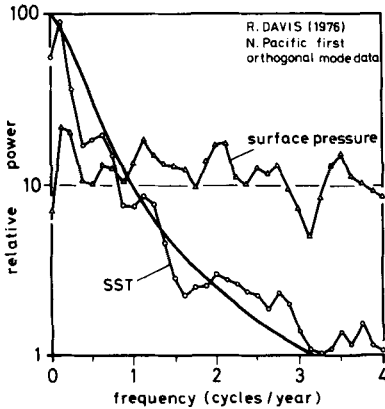
Fig. 8. Spectrum of the dominant EOF of the North Pacific SST anomaly and sea level pressure (after Davis, 1976). The smooth curve represents the predicted SST spectrum for $\lambda = (6$ month$)^{-1}$ with appropriate choice of the level of the white input spectrum.

forcing function $v(t)$ in the lag range $\tau_x \ll t \ll \tau_y$ (see relation (1.7)) has been evaluated here simply by differentiating the integrated SST time series. The input and response correlation functions (r_{vv} and r_{TT} in Fig. 7) exhibit the structure and time scale separation assumed in the stochastic model. In this example the essentially zero-lag width of the auto-correlation function of the "atmospheric forcing" follows directly from the initially linear form of the autocorrelation function of the anomaly, and is shown simply for illustration, rather than as independent corroboration of the model. The diffusion coefficient, i.e. the rate of generation of SST anomalies, can be estimated from the slope of $[\delta y^2(t)]$ at small t: $D \approx 0.04(^\circ C)^2$ yr^{-1}. This value is smaller than at station India, but is not unreasonable, when considering that the variability of the fluxes at a fixed position should be considerably higher than the variability of the fluxes averaged over the North Pacific, to which only the longest wavelengths contribute. The feedback relaxation time for the North Pacific is of the order $\lambda^{-1} = 0.75$ year, somewhat larger than the station India value, but the 3-month time increment of Namias' time series is too coarse for an accurate calculation. Namias & Born (1974) give the correlation function calculated from monthly averages of this SST data, at lags up to 24 months. An exponential decay with $\lambda = (1$ year$)^{-1}$ provides a good fit at lags larger than 6 months, but the initial decay is faster, suggesting that the feedback process may be more complex than the single-variable equation (1.7). This could be due to other

anomaly modulating-processes such as an advection or diffusion.

An analysis of 28 years of monthly averaged North Pacific SST data (north of 20° N) has been carried out by Davis (1976). The SST anomaly fields were correlated with fields of atmospheric surface pressure anomalies. Both fields were decomposed first into their empirical orthogonal functions (EOF's). Fig. 8 shows the variance spectra of the amplitudes of the dominant first EOF of each field. An exponential decay with $\lambda = (6$ months$)^{-1}$ provides an excellent fit to the correlation function of the dominant SST mode reported by Davis (his Fig. 6). This feedback factor has been used to construct the predicted SST spectra behaviour in Fig. 8. The agreement with the observed spectrum is good throughout the whole frequency range (again, aliasing may explain the somewhat higher energy at high frequencies), and the pressure spectrum is flat, as expected for an atmospheric variable.

A direct verification of the model by comparison of the input and response energy levels is again not possible for Davis' data because of the lack of appropriate time series measurements of the spatially integrated surface heat fluxes. However, Davis calculated the cross correlation function for the amplitudes of the first EOF's of the SST and surface pressure anomaly, and this provides a rather critical test of the basic premise of the model, namely that SST anomalies represent the integral response to short-time-scale atmospheric forcing.

We assume that the amplitude of a surface pressure anomaly may be chosen in place of the anomalous surface heat flux as the atmospheric variable determining the rate of change of an SST anomaly. This is permissible if the anomalous circulation patterns associated with the pressure anomalies are correlated with anomalous heat fluxes (as was the case, for example, for the heat fluxes computed from the wind field in the simple simulation model in Section 3). The variables y and v in eq. (1.7) may then be interpreted as the amplitudes of the first EOF's of the SST and surface pressure anomaly fields, respectively (except for a proportionality factor which can be normalized to unity). Multiplication of (1.7) by $v(t - \tau)$ and averaging yields the relation

$$\frac{d}{dt} R_{yv}(\tau) = R_{vv}(\tau) - \lambda R_{yv}(\tau) \qquad (4.2)$$

for the covariance functions

$$R_{yv}(\tau) = [y(t + \tau)v(t)]$$

and

$$R_{vv}(\tau) = [v(t + \tau)v(t)]$$

Assuming white-noise atmospheric forcing $R_{vv}(\tau) = A\delta(\tau)$ and $R_{yv}(\tau) = 0$ for $\tau < 0$ (causality), the solution of equation (4.2) is given by

$$R_{yv}(\tau) = A\,e^{-\lambda\tau} \qquad \text{for } \tau > 0$$

$$= 0 \qquad\qquad \text{for } \tau < 0 \qquad (4.3)$$

The observed correlation function R_{yv} is shown in Fig. 9, upper panel. The rounding of the observed correlation function at the predicted discontinuity $\tau = 0$ can be attributed to the 1-month averaging performed on the time series prior to correlating. If the smoothing effect is included (see appendix), the theoretical curve (Fig. 9, lower panel) shows a remarkable agreement with the measured correlation function.

In summary, it appears that most of the features of mid-latitude SST anomalies can be explained by a simple model of white atmospheric forcing balanced by a stabilizing linear feedback. A more detailed quantitative analysis, including multi-component cross correlation analysis of a number of EOF's of the postulated atmospheric forcing fields and the SST response, would undoubtedly reveal many refinements of the simple picture used here. For example, the investigations of Clark
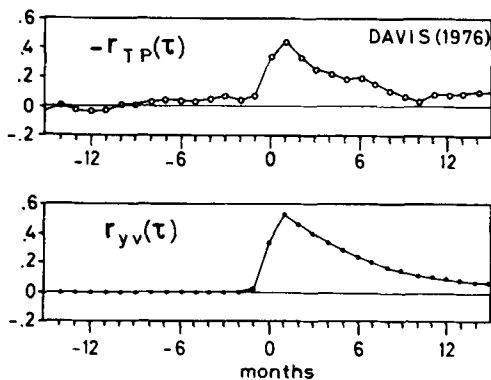

Fig. 9. Upper panel: observed correlation between the amplitude of the dominant mode of SST and sea level pressure (after Davis, 1976). Lower panel: theoretical correlation estimated from monthly averaged data for $v = (8.5 \text{ day})^{-1}$, $\lambda = (6 \text{ month})^{-1}$ (see appendix).

(1972), Gill & Niiler (1973), Gill (1975), and Emery (1976) have demonstrated that large-scale advection, local advection and upwelling due to eddies, mixed-layer deepening by wind actions and radiation flux variations can all influence the SST field significantly. A detailed regional study by Reynolds (in preparation) suggests that in regions of the ocean near strong currents or thermal fronts, oceanic processes dominate over the atmospheric forcing as the cause of SST variability. We have also ignored the seasonal modulation, which strongly affects both the low-frequency spectrum of the atmospheric forcing and the SST response (through the variable mixed-layer depth). Nonetheless, in considering long-term air–sea interaction, the concept of a time-scale separation between the two interacting media appears to yield a reasonable first-order picture as a starting point from which more accurate models can be developed.

5. Thermocline variability

As a further application of the two-scale model, we consider finally the generation of temperature variations within the near-surface thermocline. These are relatively difficult to generate by variable heating at the surface, which is largely absorbed in the mixed layer, but can be effectively excited by horizontally variable wind stresses. The divergences of the horizontal Ekman transports generated by the stresses produce vertical displacements of the isotherms, thereby inducing temperature variations at a fixed depth proportional to the vertical thermal gradient.

In general, a spatially- and time-dependent surface stress field produces two forms of response in the ocean: gravity-inertial modes, and quasi-geostrophic motions. For frequencies well below the lowest eigenfrequency of inertial-gravity modes, i.e. well below the local Coriolis frequency, the transfer function for inertial-gravity modes is essentially flat with respect to frequency, whence a white input spectrum would produce a white inertial-gravity response spectrum, rather than the observed red spectrum. The eigenfrequencies of the baroclinic quasi-geostrophic motions (Rossby waves), on the other hand, are considerably lower, of the order of a fraction of a cycle per month, and for these motions a red response spectrum may be expected.

The response of a stratified ocean subject to different forms of forcing has been studied in various contexts by many authors. A general decomposition of the forcing functions and response into inertial-gravity and geostrophic motions using projection operators is given, for example, in Hasselmann (1970). In the linear, f-plane approximation, the rate of change of the quasi-geostrophic component of the displacement ζ (relative to the free surface) of an isotherm immediately below the Ekman layer satisfies the simple "Ekman pumping" equation

$$\frac{\partial \zeta}{\partial t} = \frac{(\nabla \wedge \mathbf{S})_3}{\rho^w f} \tag{5.1}$$

where S is the stress applied at the surface and f the Coriolis parameter. (Equation (5.1) is normally derived from the continuity equation $\partial\zeta/\partial t = \nabla \cdot \mathbf{M}$ and the geostrophic relation $f \wedge \mathbf{M} = \mathbf{S}$ for the vertically integrated mass transport M of a quasi-stationary Ekman layer, but is in fact valid rigorously for the quasi-geostrophic component of the response in the f-plane, independent of the assumption of quasi-stationarity.) If the barotropic mode, which yields a negligible contribution to the near-surface isothermal displacement, is excluded, the β-plane restoring forces can be neglected to first order for time scales up to several months, and the appropriate f-plane equation (5.1) then reduces to the basic form (1.3) of a stochastically driven system without feedback.

The generation of thermocline displacements according to (5.1) was investigated in an experiment, using the atmospheric model of Section 2 to simulate the wind forcing through the bulk relation $\mathbf{S} = C_D P_a |\mathbf{U}|\mathbf{U}$, with $C_D = 1.5 \cdot 10^{-3}$. The wind stress was first constructed at each grid point, and its curl was then taken in the Fourier domain using the fast Fourier Transform method. The power spectrum of simulated wind-stress curl is approximately white at low frequencies, as other atmospheric spectra, with a spectral level of the order of 10^{-9}–10^{-10} dyn^2 cm^{-6}/Hz (10^{-7}–10^{-6} Newton^2 m^{-6}/Hz). The spatially averaged r.m.s. Ekman suction velocity is approximately 10^{-5} m s^{-1}.

Fig. 10 shows the computed power spectrum of thermocline vertical displacement at a typical location ($x = 0$, $y = L_y/3$). The associated white-noise level of the input spectrum in this case is $4 \cdot 10^{-10}$ dyn^2 cm^{-6}/Hz, which corresponds to a
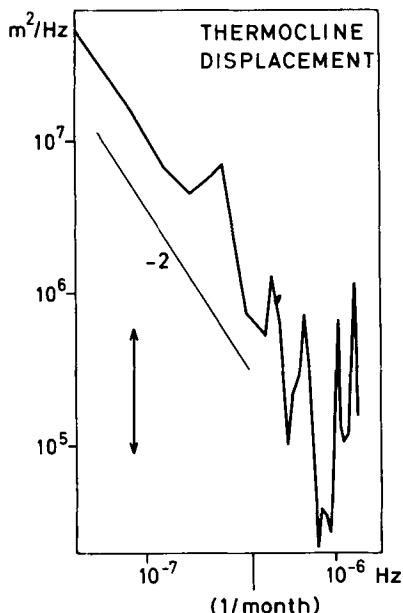

Fig. 10. Spectrum of simulated thermocline displacements at $x = 0$, $y = L_y/3$. The arrows indicate the 80% confidence interval.

diffusion coefficient $D = 63$ m^2 year^{-1}. Thus in the absence of feedback, the random short-time forcing by Ekman pumping would produce a r.m.s. vertical displacement of 11 m in a year.

However, it is possible that our atmospheric model strongly underestimates the variance spectrum of the wind-stress curl. Observations at Bermuda (Wunsch, 1972) suggest that the white-noise level of the wind-stress spectrum may be nearly one order of magnitude larger than in the model. Furthermore, the wavenumber spectrum of the simulated wind-stress curl shows a maximum contribution to the variance near wavenumber 5, which corresponds to a dominant wave length of 2500 km (Fig. 2). The strong decrease of the spectrum at higher wavenumbers is probably unrealistic and may be attributed to the large coefficient of dissipation and the truncation of the model at wavenumber 8.

Dimensional arguments suggest in fact that if the wind kinetic energy decays as k^{-3} (or less) in the enstrophy inertial range, the wind-stress curl spectrum should decay as k^{-1} (or less), so that scales not represented in our atmospheric model are likely to contribute significantly to the wind-stress curl variance. This is in agreement with the
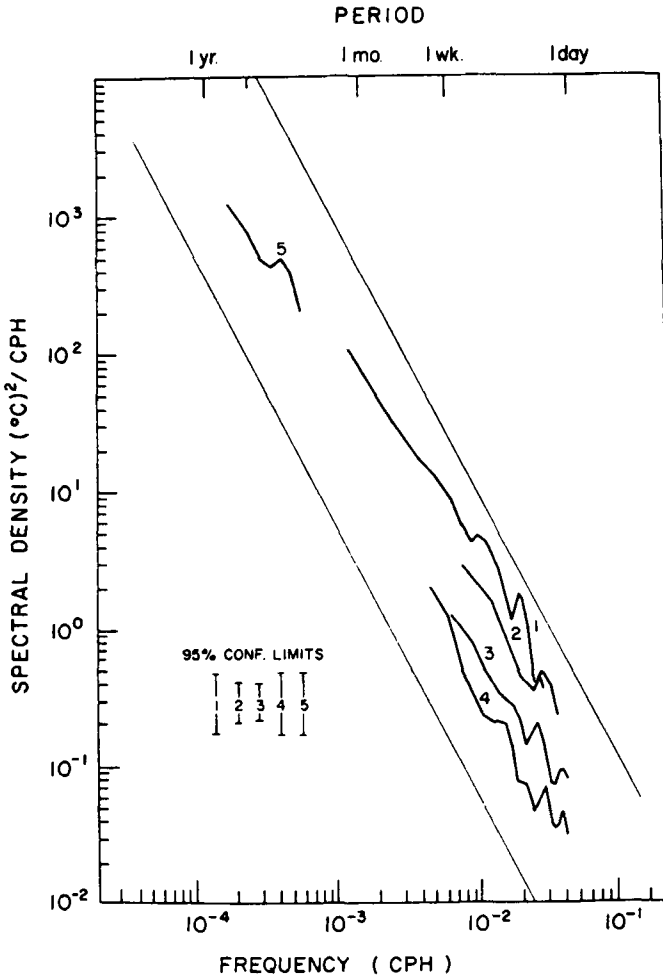
PERIOD

Fig. 11. Spectra of temperature variations in the seasonal thermocline (from Bernstein & White, 1974). Data are from various stations in the mid-Pacific between 30N and 43N at depths of 150 m (1–4) and 200 m (5). Frequency slopes of −2 are indicated.

recent work of Saunders (1976), who showed that the curl of the wind stress estimated from long-term averaged wind data was underestimated by a factor one half when computed from a 5° square grid as compared with a 1° square grid.

Fig. 10 may be compared with the spectra of temperature variations measured at various stations in the North Pacific at 150 and 200 m depth within the thermocline by Bernstein & White (1974), Fig. 11. Although the exact form of the spectrum is uncertain due to the composite nature of the data, the general trend is consistent with a ω^{-2} power law. Taking a typical thermal stratification of $5 \cdot 10^{-2}$ °C/m (cf. Bernstein & White,

1974, Fig. 8) and the Coriolis parameter for the latitude 40°, the average spectrum $F_T(\sigma) = 10^{-4} \sigma^{-2}$ (°C)^2/cph (σ = frequency in cph) of the thermocline temperature variation T shown in Fig. 14 corresponds to a spectrum of thermocline displacement $F_{\zeta\zeta} \approx 10^{-5}\nu^{-2}$ m^2 s^{-2}/Hz (ν in Hertz). This is about two orders of magnitude larger than the model data.

Another example of observed thermocline variability can be found in Fig. 16 of Wunsch (1972), which shows the variance spectra of temperature fluctuations at 100 meters depth at the Panulirus station in Bermuda. The spectrum decreased approximately as ω^{-2} for periods ranging between

1 month and 1 year and begins to flatten for periods longer than about 1 year. The energy level of the temperature spectrum is similar to that in the North Pacific, but the corresponding displacement spectrum is difficult to estimate, since seasonal variations of the vertical temperature gradient are very pronounced at this depth (cf. Schröder & Stommel, 1969).

However, the equivalent displacement spectra of both Bernstein-White and Wunsch are clearly considerably higher than the spectra simulated by the model. Taking a wind stress white-noise level of $5 \cdot 10^5$ dyne^2 cm^{-4}/Hz (estimated from Wunsch, 1972), the North Pacific data require that most of the wind-stress variance would need to be concentrated around wave lengths as short as 220 km in order to produce the observed thermocline displacements by Ekman pumping. Bernstein & White (1974) suggest, in fact, that the North Pacific thermocline variability is caused by internal baroclinic eddies, rather than wind forcing. It should be noted, however, that the examples of thermocline displacement spectra discussed here may not be very representative for other oceanic regions. Dantzler (1976) showed, for example, that there are large areas in the North Atlantic where the r.m.s. depth displacement of the 15 °C isotherm (at depths ranging from 100 to 500 m) is at least a factor 4 smaller than near Bermuda.

In summary, it remains an open question whether variability in the seasonal thermocline can be explained by atmospheric forcing, despite the agreement of the shape of the temperature frequency spectrum of a white-noise atmospheric forcing model. This question can be resolved only by a more detailed analysis of the wavenumber spectrum of the wind-stress curl, particularly in the region of high wavenumbers. But it can be concluded that at all events local atmospheric forcing should be regarded as a serious candidate for the origin of variability in the seasonal thermocline (and possibly below) in certain regions of the ocean.

6. Conclusion

With regard to SST variability it has been shown that in mid-ocean regions away from intense currents or thermal fronts the principal statistical properties of SST anomalies can be explained by a simple model in which the atmosphere acts as a white-noise generator and the ocean as a first-order Markov integrator of the atmospheric input.

The mechanism was demonstrated numerically by a Monte-Carlo simulation, using an idealized two-dimensional model of atmospheric turbulence, and was verified independently by measurements.

According to this picture, the evolution of SST anomalies is unpredictable, except that, once generated, they tend to decay with an e-folding time of the order of $\frac{1}{2}$ year. The evolution of the anomalies is independent of any feedback with the atmosphere.

It should be stressed, however, that we have presented only a first-order picture and have ignored important effects such as the seasonal modulation, interactions within the ocean and higher-order anomaly-pattern interactions. Our analysis was based either on single-station data, spatially averaged data or on the interaction between the dominant first EOF's of SST and atmospheric pressure anomaly. A more detailed analysis using a more sophisticated model and a more extensive data base may well reveal higher order feedback processes of practical significance for long-range weather forecasting.

The analysis of variability in the seasonal thermocline provided some evidence, from the general structure of the frequency spectra, of white-noise atmospheric forcing, but a quantitative comparison of the input and response spectra remained inconclusive because of inadequate information on the wavenumber-frequency spectra of the wind-stress curl. Since the atmospheric forcing may be expected to lie in the same range of the wavenumber spectrum as the oceanic mesoscale eddies, which contain the major portion of the kinetic energy of the ocean, it is important to clarify whether a significant part of the eddy energy near the surface (and possibly deeper) could be generated by local atmospheric forcing. We conclude that, on the basis of present evidence, this mechanism must be considered as a possible important source of mesoscale eddy energy in certain regions of the ocean and should be investigated further.

7. Acknowledgements

8. Appendix

Effect of smoothing on the correlation between climate and weather variables

Here we generalize the result (4.3) to include a finite correlation of the atmospheric forcing and the effect of data smoothing. Following Munk (1960) and Leith (1973) we represent the weather variable $v(t)$ in eq. (1.7) by a first-order Markov process, whose autocorrelation is given by

$$r_{vv}(\tau) = e^{-v|\tau|} \tag{A1}$$

The precise form of r_{vv} is not critical. Equation (4.2) and the corresponding equation for the covariance function $R_{yy}(\tau) = [y(t + \tau)y(t)]$ then yield the correlation functions

$$r_{yv}(\tau) \approx \left(\frac{\lambda}{v}\right)^{1/2} e^{v\tau} \qquad \text{for } \tau \leqslant 0 \tag{A2}$$

$$\approx \left(\frac{\lambda}{v}\right)^{1/2} e^{-\lambda\tau}(2 - e^{-v\tau}) \qquad \text{for } \tau \geqslant 0$$

$$r_{yy}(\tau) \simeq e^{-\lambda|\tau|} \tag{A3}$$

where we have assumed $\lambda \ll v$, consistent with our two-time scale approximation.

If the anomaly data is time averaged over an interval T, the covariance function $R_{\alpha\beta}(\tau)$ between the smoothed variables α and β is given by

$$\overline{R}_{\alpha\beta}(\tau) = \frac{1}{T^2} \int_{-T/2}^{T/2} dt' \int_{-T/2}^{T/2} dt'' R_{\alpha\beta}(t' + \tau - t'') \tag{A4}$$

For an averaging time T in the interval $v^{-1} \ll T \ll \lambda^{-1}$, one finds, after some algebra

$$\overline{r}_{vv}(nT) = 1 \qquad n = 0$$

$$\simeq \frac{e^{vT} e^{-v|nT|}}{2(vT-1)} \qquad n = \pm 1, \pm 2, \dots \tag{A5}$$

$$\overline{r}_{yy}(n) \simeq e^{-\lambda|nT|} \qquad n = 0, \pm 1, \pm 2,\dots \tag{A6}$$

$$\overline{r}_{yv}(n) \simeq \left(\frac{\lambda v T^2}{2(vT-1)}\right)^{1/2} \frac{e^{(n+1)vT}}{v^2 T^2} \qquad n = -1, -2, \dots$$

$$\simeq \left(\frac{\lambda v T^2}{2(vT-1)}\right)^{1/2} \qquad n = 0$$

$$\simeq \left(\frac{2\lambda v T^2}{vT-1}\right)^{1/2} e^{-n\lambda T} \qquad n = 1, 2, \dots \tag{A7}$$

Relation (A5) is an approximate form of the relation (5) given by Munk (1960) in his discussion of the increased persistence of atmospheric variables by smoothing. Relation (A6) shows that the correlation function of the climate variable is not affected by smoothing, as expected. However, the cross correlation between the climate and weather variable is increased considerably through smoothing. Also, the shape of the curve is modified.

The increase of the correlation between climate and weather variables by smoothing can be readily understood in terms of the variance spectra. Equations (1.5), (1.6) and (1.9) show that the climate response is driven by the low-frequency part of the input spectrum. By low-pass filtering the atmospheric input the main part of the spectrum which does not contribute to the climatic response is removed, whereas the essential low-frequency region of the input spectrum is left unchanged. Thus the residual input signal will exhibit a much higher correlation with the climatic response than the unfiltered input.

For $v = (4 \text{ day})^{-1}$ and $\lambda = (6 \text{ month})^{-1}$, representative of the weather and SST anomalies respectively, the zero-lag unsmoothed correlation $r_{Tv}(0)$ is 0.15 (similar to the value reported by Salmon & Hendershott (1976)), and the correlation function has a maximum of 0.27 when the weather variable leads the SST by 12 days. If monthly averaged data are used, the predicted zero-lag correlation is $\overline{r}_{Tv}(0) = 0.31$, and a maximum correlation of 0.52 occurs when v leads T by one month. If seasonal averages are used, even higher correlations result, 0.5 at zero lag and a maximum of 0.6 at lag one (one season). This is consistent with the high correlation factors repor-

ted for time-averaged data, for example by Namias (1969). Equation (A7) was used to construct the predicted curve in the lower panel of Fig. 9 (Section 4), taking $v = (8.5 \text{ day})^{-1}$ in accordance with the value quoted by Davis (1976) for the 1st EOF of the North Pacific surface pressure anomaly.

REFERENCES

Bernstein, R. L. & White, W. B. 1974. Time and length scales of baroclinic eddies in the central North Pacific ocean. *J. Phys. Oceanogr. 4*, 613–624.

Bjerknes, J. 1966. A possible response of the atmospheric Hadley circulation to equatorial anomalies of ocean temperature. *Tellus 28*, 820–828.

Byshev, V. I. & Ivanov, Y. A. 1969. The time spectra of some characteristics of the atmosphere above the ocean. *Izvestiya Akademii nauk SSSR 5*, 17–28.

Chervin, R. M., Washington, W. M. & Schneider, S. H. 1976. Testing the statistical significance of the response of the NCAR General Circulation Model to North Pacific ocean surface temperature anomalies. *J. Atmos. Sciences 33*, 413–423.

Clark, N. E. 1972. Specification of sea surface temperature anomaly patterns in the eastern North Pacific. *J. Phys. Oceanogr. 2*, 391–404.

Davis, R. E. 1976. Predictability of sea surface temperature and sea level pressure anomalies over the North Pacific ocean. *J. Phys. Oceanogr. 6*, 249–266.

Dantzler, H. L. Jr. 1977. Potential energy maxima in the tropical and subtropical North Atlantic. *J. Phys. Oceanogr.* (submitted to).

Denman, K. L. 1973. A time-dependent model of the upper ocean. *J. Phys. Oceanogr. 3*, 173–184.

Emery, W. J. 1976. The role of vertical motion in the heat budget of the upper Northeastern Pacific Ocean. *J. Phys. Oceanogr. 6*, 299–305.

Frost, M. R. 1975. Stress, evaporative heat flux and sensible heat flux distributions of the North Atlantic (mid-latitude) and their contribution to the production of large scale sea surface temperature anomalies, Master thesis, Southampton University.

Gill, A. E. 1975. Evidence for mid-ocean eddies in weather ship records. *Deep-Sea Res. 22*, 647–652.

Gill, A. E. & Niiler, P. P. 1973. The theory of the seasonal variability in the ocean. *Deep-Sea Res. 20*, 141–177.

Hasselmann, K. 1970. Wave-driven inertial oscillations. *Geophys. Fluid Dyn. 1*, 463–502.

Hasselmann, K. 1976. Stochastic climate models. Part I, theory. *Tellus 28*, 473–485.

Kao, S. R. & Wendell, L. L. 1970. The kinetic energy of large-scale atmospheric motion in wavenumber-frequency space: I. Northern Hemisphere. *J. Atmos. Sci. 27*, 359–375.

Kraus, E. B. & Morrison, R. E. 1966. Local interactions between the sea and the air at monthly and annual time scales. *Quart. J. Royal Meteor. Soc. 92*, 114–127.

Kraus, E. B. & Turner, J. S. 1967. A one-dimensional model of the seasonal thermocline: II. The general theory and its consequences, *Tellus 19*, 98–106.

Kruse, B. 1975. Untersuchung großskaliger nicht-linearer Wellenwechselwirkungen mit einem numerischen spektralen Einschichtenmodell, Diplomarbeit, Universität Hamburg.

Leith, C. E. 1973. The standard error of time-average estimates of climatic means. *J. Applied Meteorology 12*, 1066–1069.

Lemke, P. 1977. Stochastic climate models, Part 3. Application to zonally averaged energy models. To appear in *Tellus.*

Lilly, D. K. 1972. Numerical simulation studies of two-dimensional turbulence: I. *Geophys. Fluid Dyn. 3*, 289–319.

Mitchell, J. M. Jr. 1966. Stochastic models of air–sea interaction and climatic fluctuation. (Symp. on the Arctic Heat Budget and Atmospheric Circulation, Lake Arrowhead, Calif., 1966). Mem. RM-5233-NSF, The Rand Corp., Santa Monica.

Munk, W. H. 1960. Smoothing and persistence. *J. Atmosph. Sci. 17*, 92–93.

Namias, J. 1959. Recent seasonal interactions between North Pacific waters and the overlying atmospheric circulation. *J. Geophys. Res. 64*, 631–646.

Namias, J. 1969. Seasonal interactions between the North Pacific ocean and the atmosphere during the 1960's. *Month. Weath. Rev. 97*, 173–192.

Namias, J. 1975. Stabilization of atmospheric circulation patterns by sea surface temperature. *J. Mar. Res. 33*, Suppl., 53–60.

Namias, J. & Born, R. M. 1974. Further studies of temporal coherence in the North Pacific sea surface temperatures. *J. Geophys. Res. 79*, 893–894.

Niiler, P. P. 1975. Deepening of the wind-mixed layer. *J. Marine Res. 33*, 405–422.

Rhines, P. B. 1975. Waves and turbulence on a beta-plane. *J. Fluid Mech. 69*, 417–443.

Rowntree, P. R. 1976. Response of the atmosphere to a tropical Atlantic ocean temperature anomaly. *Quart. J. Roy. Met. Soc. 102*, 607–625.

Salmon, R. & Hendershott, M. C. 1976. Large scale air-sea interactions with a simple general circulation model. *Tellus 28*, 228–242.

Saunders, P. M. 1976. On the uncertainty of wind stress curl calculations. *J. Marine Res. 34*, 155–160.

Schroeder, E. & Stommel, H. 1969. How representative is the series of monthly mean conditions off Bermuda? in *Progress in Oceanography*, edited by M. Sears, pp. 31–40, Pergamon, New York.

Shukla, J. 1975. Effect of arabian sea-surface temperature anomaly on Indian summer monsoon: a

numerical experiment with the GFDL model. *J. Atmos. Sci. 32*, 503–511.

Taylor, G. I. 1921. Diffusion by continuous movements. *Proc. Lond. Math. Soc. 20*, 196.

Thompson, R. O. R. Y. 1976. Climatological numerical

models of the surface mixed layer of the ocean. *J. Phys. Oceanogr. 6*, 496–503.

Wunsch, C. 1972. Bermuda sea level in relation to tides, weather, and baroclinic fluctuations. *Rev. Geophys. Space Phys. 10*, 1–49.

СТОХАСТИЧЕСКИЕ МОДЕЛИ КЛИМАТА. ЧАСТЬ 2.
ПРИМЕНЕНИЯ К АНОМАЛИЯМ ТЕМПЕРАТУРЫ ПОВЕРХНОСТИ МОРЯ И ИЗМЕНЧИВОСТИ ТЕРМОКЛИНА.

Концепция стохастических моделей климата, развитая в части I этой серии (Хассельман, 1976) применяется для изучения низкочастотной изменчивости верхнего слоя океана. Показано, что крупномасштабные долгопериодные аномалии температуры поверхности моря (ТПМ) могут быть естественным образом объяснены как реакция верхних слоев океана на короткопериодное воздействие атмосферы. Спектр белого шума атмосферного воздействия приводит для реакции к спектру красного шума, с концентрацией большей части дисперсии в очень длинных периодах. Без учета стабилизирующей отрицательной обратной связи реакция океана была бы нестационарной и полная дисперсия ТПМ неограниченно росла бы со временем. С учетом отрицательной обратной связи реакция является асимптотически стационарной. Эти эффекты иллюстрируются с помощью численных экспериментов с

очень простой моделью океана и атмосферы. Модель воспроизводит принципиальные особенности и порядки величин наблюдаемых аномалий ТПМ в средних широтах. Независимая поддержка модели стохастического воздействия дается прямым сравнением спектров наблюдаемых потоков тепла и скрытой теплоты со спектрами аномалий ТПМ, а также сравнением структуры функций взаимной корреляции атмосферного давления у поверхности и полей аномалий ТПМ. Далее численная модель используется для моделирования аномалий в приповерхностном термоклине путем экмановской накачки, вызываемой ротором напряжения ветра. Результаты показывают, что короткопериодное атмосферное воздействие следует рассматривать как возможный источник происхождения крупномасштабной доигопериодной изменчивости в сезонном термоклине.